

A spatially resolved model for pressure filtration of edible fat slurries

Van den Akker, Harry E.A.; Hazelhoff Heeres, Doedo P.; Kloek, William

DOI

[10.1002/aic.17307](https://doi.org/10.1002/aic.17307)

Publication date

2021

Document Version

Final published version

Published in

AIChE Journal

Citation (APA)

Van den Akker, H. E. A., Hazelhoff Heeres, D. P., & Kloek, W. (2021). A spatially resolved model for pressure filtration of edible fat slurries. *AIChE Journal*, 67(10), Article e17307. <https://doi.org/10.1002/aic.17307>

Important note

To cite this publication, please use the final published version (if applicable). Please check the document version above.

Copyright

Other than for strictly personal use, it is not permitted to download, forward or distribute the text or part of it, without the consent of the author(s) and/or copyright holder(s), unless the work is under an open content license such as Creative Commons.

Takedown policy

Please contact us and provide details if you believe this document breaches copyrights. We will remove access to the work immediately and investigate your claim.

A spatially resolved model for pressure filtration of edible fat slurries

Harry E. A. Van den Akker^{1,2}  | Doedo P. Hazelhoff Heeres¹ | William Kloek³

¹Transport Phenomena Group, Department of Chemical Engineering, Faculty of Applied Sciences, Delft University of Technology, Delft, Netherlands

²Bernal Institute, School of Engineering, University of Limerick, Limerick, Ireland

³FrieslandCampina, Amersfoort, The Netherlands

Correspondence

Harry E. A. Van den Akker, Transport Phenomena Group, Dept. of Chemical Engineering, Faculty of Applied Sciences, Delft University of Technology, Delft, Netherlands.
Email: harry.vandenakker@ul.ie

Abstract

A spatially resolved one dimensional pressure filtration model was developed for a slurry of edible fat crystals. The model focuses on the expression step in which a cake is compressed to force the liquid through a filter cloth. The model describes the local oil flow in the shrinking cake modeled as a porous nonlinear elastic medium existing of two phases, viz. porous aggregates and interaggregate liquid. Conservation equations lead to a set of two differential equations (vs. time and vs. a material coordinate ω) for two void ratios, which are solved numerically by exploiting a finite-difference scheme. A simulation with this model results in a spatially resolved cake composition and in the outflow velocity, both as a function of time, as well as the final solid fat contents of the cake. Simulation results for various filtration conditions are compared with experimental data collected in a pilot-plant scale filter press.

KEYWORDS

cake consolidation, fat agglomerates, food processing, numerical simulation, pressure filtration

1 | INTRODUCTION

Pressure filtration/expression is a process aimed at separating two phases such as in thickening of minerals and oil sands tailings in the mining industry^{1,2} and of coal reuse slurries,³ in dewatering of sludge in waste water treatment⁴ or of papermaking pulp fibers,⁵ in expressing rubber seed oil from dehulled rubber seeds,⁶ and in expressing biological material in the food and beverage industry such as sugar beet pulp,^{7,8} cocoa nibbs⁹ or oil seeds.^{10,11} In several of the above applications, the dispersed phase just consists of solid hard particles. The classical models in the literature deal with solid particles as well, where compression by an external force may affect the network of the particles rather than the shape or size of the particles although particles may ultimately break (fracture) into smaller fragments. In other cases, the dispersed particles may contain liquids which may be harvested by expressing the particles themselves.

This paper deals with pressure filtration/expression of edible fat crystal aggregates, with a diameter in the order of 100 μm (see Figure 1), to be separated from an oil-like mother liquor. A characteristic feature of this process is that the soft loose aggregates not only are immersed in the oil but also contain the oil. The oil should therefore not only removed from the interaggregate space but also from the aggregates themselves. To this end, an external pressure is applied to the aggregates-liquor mixture. Our pressure filtration/expression is carried out in a membrane filter press which essentially comprises the same steps as the flexible-membrane plate-and-frame filter press cycle shown in Figure 1 of the paper by Stickland et al.¹² A specific pressure-time profile is imposed with the view of optimizing or improving the filtration and expression process in terms of both filtration time and final solid fat contents of the cake. We developed a one-dimensional (1D) numerical model with the view to such optimizations.

This is an open access article under the terms of the Creative Commons Attribution-NonCommercial-NoDerivs License, which permits use and distribution in any medium, provided the original work is properly cited, the use is non-commercial and no modifications or adaptations are made.

© 2021 The Authors. *AIChE Journal* published by Wiley Periodicals LLC on behalf of American Institute of Chemical Engineers.

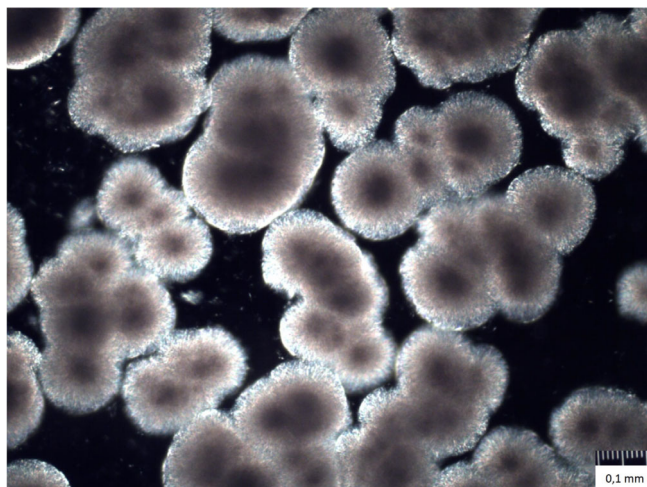


FIGURE 1 Image of a slurry with spherulitic fat crystal aggregates; the scale in the lower right corner is 100 μm [Color figure can be viewed at wileyonlinelibrary.com]

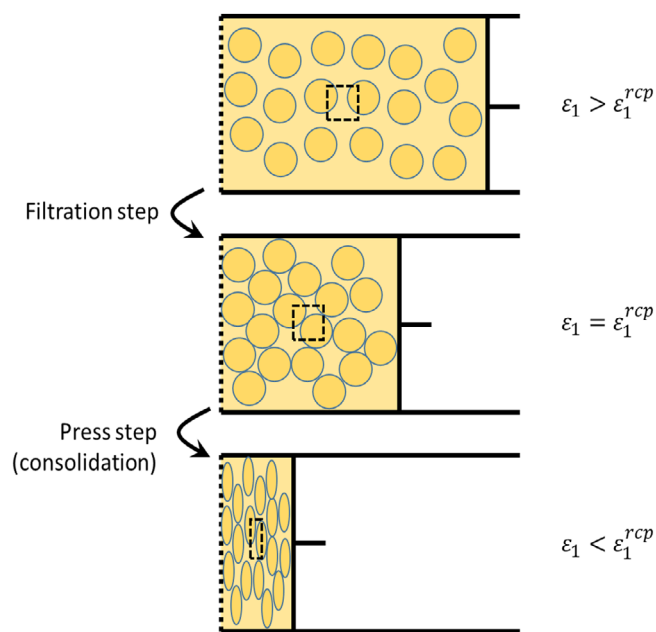


FIGURE 2 The two stages of a filtration and expression process separated by the random close packing (see the middle figure) representing the transition from filtration to expression [Color figure can be viewed at wileyonlinelibrary.com]

In a somewhat simplified version of this filtration process, a cake is compressed one-sided by applying a load (see Figure 2 top) to force the liquid through a filter cloth at the other side. At the start of this pressure assisted filtration process, the cake consists of loosely packed porous crystal aggregates containing oil while surrounded by a continuous oil phase (see again Figure 2 top). When the pressure is increased, the cake with the aggregates is compressed to force the oil out of the loose network as well as out of the aggregates and to flow through the consolidating network, later on turning into a cake,

towards the filter cloth at the other end, as illustrated in the middle and bottom panels of Figure 2. This paper describes a novel model for describing this 1D expression process in terms of temporally and spatially resolved porosities of aggregates and cake, resulting in a time-dependent oil flux through the cloth out of the cake.

The topic of filtration goes back to the 1856 paper by D'Arcy on the flow of water through sands and sand stones, and was then further investigated in the 1920s and 1930s in papers by Terzaghi,¹³ Ruth¹⁴ and Carman.¹⁵ The seepage, or infiltration, of a fluid in the underground, such as (fractured) rocks, was the topic of a 1960 paper by Barenblatt and Zheltov.¹⁶ It was the start of a long series of papers on models of increasing complexity (particularly dual-porosity dual-permeability models) on the transient flow of fluids through fractured reservoirs relevant to the oil industry.¹⁷ The latter models are not particularly relevant to the current case of interest.

With respect to cake filtration/expression, Ruth¹⁴ referred to the "widespread idea that the mechanism of filtration is one of such extreme variability that the engineer may perhaps never hope to find law and order in its operation." Not surprisingly, the topic has challenged many experimentalists and modeling researchers: the review by Olivier et al.¹⁸ in 2007 already cites 159 papers. The topic was also covered in two books by Tien^{19,20} and also a recent paper by Mahwachi and Mihoubi²¹ summarizes the conventional equations. A thorough review of the topic is beyond the scope of this paper however. We will just focus on our novel filtration/expression model and on where it differs from earlier models.

The basic filtration equations due to Ruth,¹⁴ still in use today, relate filtrate volume as a function of time to pressure drop (over filter cake and filter medium) in terms of specific resistance and volume of the filter cake. Terzaghi,¹³ interested in consolidation of clay due to a load on top, assumed that layer (or cake) thickness, compressibility and permeability remain constant. Tiller et al.²² combined Darcy's law for the flow through a porous medium with the notions of solids pressure and consolidation, which not only are relevant to soil mechanics but also to the filter cake of current interest. The common models for constant pressure filtration lead to a quadratic relationship between filtration time and filtrate volume.^{23,24} Stickland et al.¹² reviewed deviations from such a quadratic behavior. Owolarafe et al.²⁵ reported about a model for expressing oil from oil palm fruit on the basis of Darcy's law for a cylindrical geometry and supplemented with several empirical relations.

Shirato et al.²⁶ distinguished between primary consolidation and secondary consolidation (due to creep), releasing the assumption of instantaneous mechanical equilibrium made in the Terzaghi model. Venter et al.⁹ and Abduh et al.⁶ successfully applied the Shirato model to the expression of cocoa liquor from finely grinded cocoa nibs and of rubber seed oil from dehulled rubber seeds, respectively. Buttersack²⁷ developed a two-zone model. In the first zone, with a void fraction between the initial value and a threshold value, the solids-solids interaction is ignored. When and where the water content falls short of the threshold value, a second zone consisting of an solids network with increasing elasticity modulus is formed. Filtration and consolidation are not regarded as subsequent stages, but are assumed to

occur alongside each other to an extent varying in time. This elastic network may be associated with the dense sphere packing for a filter cake composed of spherical particles. His model gave satisfactory results for press-dewatering of materials such as protein, sawdust, semi-solid clay and sugar-beet tissue. Ramarao et al.⁵ presented a dewatering model for a fibrous cake containing macro-pores (in between the fibers) and micropores (inside the fibers).

2 | MORE ADVANCED MODELING

In an increasingly sophisticated approach, Lanoisellé et al.²⁸ studied pressure filtration of cellular material (as applied in various agro-food processes) and pointed out that for cellular filter cakes the expression step is much more complex than for mineral cakes. This was already appreciated by Mrema and McNulty¹⁰ who built their model of oil expression from oil seeds upon three elements: (1) the oil flow through the cell wall pores; (2) the oil flow in the interkernel voids; and (3) consolidation of the oil seed cake. More or less similarly, Lanoisellé's "Liquid-Containing Biporous Particles Expression Model" describes liquid transport within a network of three different volume fractions of a cake: extra-particle, extracellular and intracellular with different behavior. The resulting system of three complex partial differential equations is solved for a constant imposed pressure and allows for the calculation of the total layer settlement as well as the deformation of the separate extra-particle, extracellular and intracellular volumes. The more recent paper by Petryk and Vorobiev²⁹ uses a similar model to describe the expression of soft plant materials. However, in both papers, the cellular material properties are very different from those of the fat crystal aggregates of current interest while the pressures applied are much higher than in a filtration process of edible fat crystals.

Kamst et al.^{30,31} modified the old empirical nonlinear viscoelastic model due to Nutting (1921) to describe the compressibility of palm oil filter cakes which are highly compressible and viscoelastic. In addition, these authors used a strain hardening model to accommodate the effect of the pressure history of the filter cake. These models, combined with an empirical relation for the permeability, made up a novel expression model. The numerical implementation was done with a finite difference scheme exploiting an exponential grid and a variable time step. This model ignores the Kozeny–Carman equation, just like Tien and Ramarao³² question the applicability of the Kozeny–Carman equation to consolidating cakes, after Grace already did the same in 1953.

Kamst's expression model predicts a pressure of 4.7 bar above which the solid fat content (SFC) does not increase anymore. Another finding of the Kamst model—relevant for the current study—was that applying a constant pressure, compared to a time-dependent pressure profile with the same end pressure, does not lead to a higher eventual SFC, although the option of applying different pressure–time profiles was not studied. Furthermore, some of Kamst's tests and simulations exceed the time scales of our process by an order of magnitude. Most importantly, however, their model ignores the biporous nature of the

filter cake (in their case, palm oil), while the double porosity is a very attractive element of Lanoisellé's model, given the fat crystal slurries of current interest.

3 | EDIBLE FAT CRYSTAL AGGREGATES

After filling the filter chamber (during which some liquid already may leave the chamber), an external pressure (or load) is applied (at the right-hand side in Figure 2, top) to start the first step of filtration in which the interaggregate porosity is still smaller than the random close packing ε_{rcp} ($=0.64$). When pressurization continues, the stage of expression or consolidation is entered in which the aggregates get compressed and squeezed (see Figure 2, bottom). The expression model we developed and describe in this paper builds on the above three elements already described by Mrema and McNulty¹⁰ and on Lanoisellé's biporous model²⁸ while considering the typical behavior and physical properties of the edible fat crystal aggregates of current interest and the pressure levels of the pertinent expression process. The crystal aggregates will therefore be considered as additional sources of oil when squeezed in the expression stage.

Our type of edible fat crystal aggregates largely exhibits elastic behavior upon compression. In the initial phase of the filtration, that is, at very low strains (in the range of 0.001–0.01), some structure breakdown may occur. These low strains, however, fall outside the range of our model calculations. We measure the Young's modulus of our aggregate network, being a measure for its elastic behavior, during compression at deformations (strains) between 0.01 and 0.3, values representative of the conditions during our filtration/expression process. The Young's modulus of the network of aggregates is directly related to the modulus of a single aggregate. Therefore, we ignore plasticity (permanent deformation) in our model and assume that the agglomerates stay intact, that is, do not break up when squeezed. We do take some energy dissipation into account in the expression phase, as we will show further on that our expression model is a rheological model composed of two dashpots in series parallel to a spring. The spring is due to the Young's modulus, the dashpots representing the friction.

For the sake of simplicity, we will consider a flat cake with (essentially) 1D transport of liquid, as a result of a unidirectional pressure applied at the right-hand side of the cake, towards a filter cloth at the left-hand side through which the liquid leaves the cake.

4 | SOME BASIC CONCEPTS

The volume reduction of a fat crystal aggregate upon compression, or squeezing, implies the aggregate must release oil, as the intrinsic densities of the oil and fat may be taken constant. On the analogy of Lanoisellé's biporous model,²⁸ we therefore distinguish between the interaggregate liquid (surrounding the crystal aggregates) with volume fraction ε_1 and the liquid contained inside the aggregates with

TABLE 1 Summary of the conventional definitions of solidosities and void ratios

| | |
|--|---|
| Interaggregate solidosity (or packing fraction) | $s_1 = 1 - \varepsilon_1$ |
| Aggregate solidosity | $s_2 = 1 - \varepsilon_2$ |
| Total solidosity | $s = s_1 s_2$ |
| Interaggregate void ratio | $e_1 = \varepsilon_1 / s_1 = \varepsilon_1 / (1 - \varepsilon_1)$ |
| (Intra)aggregate void ratio | $e_2 = \varepsilon_2 / s_2 = \varepsilon_2 / (1 - \varepsilon_2)$ |
| Total void ratio | $e = (1 + e_1)(1 + e_2) - 1$ |

porosity ε_2 . We presume that the pores inside the aggregates are smaller than the interaggregate pores by at least an order of magnitude.

We adopt the common definitions of solidosities (denoting the compliments of the above liquid volume fractions) and void ratios: see Table 1. Note that the (intra)aggregate void ratio e_2 denotes the aggregate pore volume per solid fat volume. All volume fractions, solidosities and void ratios vary spatially and in time. Our model aims at resolving them.

The motion of the aggregates during filtration/expression complicates the numerical solution of the diffusion equations—see e.g., Smiles.³³ Therefore, we adopt the conventional approach as used by for example, Terzaghi,¹³ Sørensen et al.,³⁴ Kamst et al.³⁰ and Landman and White,²⁴ and switch to the Lagrangian or material coordinate ω , defined by

$$d\omega = s dx \quad (1)$$

where x denotes the spatial coordinate in the direction of the flow towards the cloth filter, with $x = 0$ at the high-pressure end. In the material coordinate system, the only flow is that of the liquid relative to the solids. The liquid flux passing the solids is denoted by u and is related to the linear liquid and solids velocities by

$$u = \varepsilon_1 (v_{l,x} - v_{s,x}) \quad (2)$$

In adopting this material coordinate system, we deviate from the analyses of Lanoisellé et al.²⁸ and Petryk and Vorobiev.²⁹

5 | THE EXPRESSION MODEL

Due to the distinction between interaggregate and intraaggregate oil, we need two continuity equations with, at the RHS, a source and a sink term, respectively. For the interaggregate oil, and assuming a constant liquid density, the continuity equation runs as

$$\frac{\partial \varepsilon_1}{\partial t} + \frac{\partial \varepsilon_1 v_{l,x}}{\partial x} = s_1 q \quad (3)$$

in which q at the RHS denotes the release, per aggregate volume (in s^{-1}), of interaggregate oil from the aggregates. After having divided all terms of Equation (3) by s , we can switch to the material coordinate

ω as defined in Equation (1), and by also using Equation (2), we arrive at the continuity equation

$$\frac{\partial \varepsilon_1}{\partial t} \frac{1}{s} + \frac{\partial u}{\partial \omega} = \frac{q}{s_2} \quad (4)$$

for the interaggregate oil. For the intraaggregate oil, we may drop the convective term, since, as long as the liquid stays within the aggregate pores, its velocity (relative to the solids) is zero.

$$\frac{\partial e_2}{\partial t} = -\frac{q}{s_2} \quad (5)$$

Our biporous model essentially differs from the simple single continuity equation $\partial e / \partial t = \partial u / \partial \omega$ used by Sørensen et al.³⁴ and Kamst et al.³⁰

The (local) flux u depends on the (local) pressure gradient in the liquid phase and is assumed to obey Darcy's law with permeability k . The convective term of Equation (4) is then replaced by a pressure gradient:

$$\frac{\partial u}{\partial \omega} = -\frac{1}{\mu} \frac{\partial}{\partial \omega} k_1 \frac{\partial p_l}{\partial x} = -\frac{1}{\mu} \frac{\partial}{\partial \omega} s k_1 \frac{\partial p_l}{\partial \omega} \quad (6)$$

The liquid pressure balances the stress in the deforming filter cake (see e.g., Olivier et al.¹⁸):

$$\frac{\partial p_l}{\partial x} + \frac{\partial p_s}{\partial x} = 0 \quad (7)$$

while an elastic modulus E connects the solids pressure p_s to the logarithmic strain ε_{ls} :

$$E = \frac{dp_s}{d\varepsilon_{ls}} \text{ in which } \varepsilon_{ls} = -\ln\left(\frac{\delta(t)}{\delta_0}\right) = \ln\left(\frac{1+e_0}{1+e}\right) \quad (8)$$

with δ standing for the thickness of the filter cake and the subscript 0 denoting initial values, before cake deformation sets in. By applying the chain rule twice:

$$\frac{\partial p_l}{\partial \omega} = -\frac{\partial p_s}{\partial \omega} = -\frac{\partial p_s}{\partial \varepsilon_{ls}} \frac{\partial \varepsilon_{ls}}{\partial e_1} \frac{\partial e_1}{\partial \omega} \quad (9)$$

We see that the pressure gradients may be conceived as comprising three components, viz. the variation of the solids pressure with strain as expressed by the elastic modulus, the variation of strain with void ratio denoting in this case the degree of compressibility, and the void ratio gradient. Using Equation (8) then to eliminate the first two partial derivatives on the RHS of Equation (9) and substituting Equation (9) into Equation (6) lead to

$$\frac{\partial u}{\partial \omega} = -\frac{1}{\mu} \frac{\partial}{\partial \omega} \frac{k_1 E}{(1+e_1)^2 (1+e_2)} \frac{\partial e_1}{\partial \omega} \quad (10)$$

We should realize that in a nonlinearly elastic medium the elastic modulus depends on the filter cake strain itself, that is, $E = E(e_1, e_2)$. The above manipulations eventually turn the (seemingly) convective term of Equation (4) into a diffusive term. The chain rule of Equation (9) has unraveled the process and demonstrates the separate effects of elasticity and compressibility in the effective diffusivity relative to the aggregates (due to the use of the material coordinate ω). Such a diffusive term is not uncommon: see for example, Tosun,³⁵ Sørensen et al.,³⁴ Kamst et al.,³⁰ and Olivier et al.¹⁸ As a matter of fact, the basic idea can already be found in the classical Terzaghi paper dated as early as 1923.¹³ The model of Ramarao et al.⁵ is also in terms of diffusivities but lacks the elastic behavior.

Substituting Equation (10) into Equation (4) and rewriting the solidosities s and s_2 in terms of e_1 and e_2 results in

$$\frac{\partial e_1}{\partial t} = \frac{1}{1+e_2} \left[\frac{1}{\mu} \frac{\partial}{\partial \omega} \frac{k_1 E}{(1+e_1)^2 (1+e_2)} \frac{\partial e_1}{\partial \omega} - e_1 \frac{\partial e_2}{\partial t} \right] + q \quad (11)$$

while Equation (5) can be rewritten as

$$\frac{\partial e_2}{\partial t} = - (1+e_2) q \quad (12)$$

These two coupled equations of our biporous model are very different from the double-porosity Barenblatt-Zhel'tov models¹⁷ and from those presented by Ramarao et al.⁵ as the porosity of our dispersed phase is not constant but decreases in time.

The next step is to find an expression for the release rate q in Equations (11) and (12). Different from Mrema and McNulty,¹⁰ we assume the flux out of the aggregates is Darcian, with a permeability $k_2 = k_2(e_2)$ associated with the aggregates, through the specific area $a = \delta/d_a$ for the spherulitic aggregates of constant average size d_a . The pressure gradient can be transformed as above, resulting in

$$q = \frac{\delta k_2}{d_a \mu} \left| \frac{\partial p_l}{\partial x} \right| = \frac{\delta}{\mu d_a} \frac{k_2 E}{(1+e_1)^2 (1+e_2)} \left| \frac{\partial e_1}{\partial \omega} \right| \quad (13)$$

The above Equations (11)–(13) contain the cake properties k_1 , k_2 , and E which all are dependent on the pertinent the pertinent void ratios. We need empirical correlations for these parameters. As, according to Tien and Ramarao,³² the Kozeny–Carman relation is not valid under consolidating conditions, we use the Meyer and Smith³⁶ correlation

$$k = \frac{d^2}{90} \frac{\varepsilon^{4.1}}{(1-\varepsilon)^2} = \frac{d^2}{90} \frac{e^{4.1}}{(1+e)^{2.1}} \quad (14)$$

For k_1 , we use void ratio e_1 and aggregate size d_a , while k_2 needs e_2 and the typical diameter d_c of the individual crystals that build the agglomerate. Fitting an exponential function through data for strain ε_{fs} in response to applying a constant load p_p onto a slurry for various values of p_p results in an expression of the type

$$p_p = c_1 [\exp(c_2 \varepsilon_{fs}) - 1] \quad (15)$$

Using Equation (8) then results in the expression

$$E = c_1 c_2 \exp(c_2 \varepsilon_{fs}) = c_1 c_2 \left(\frac{1+e_0}{(1+e_1)(1+e_2)} \right)^{c_2} \quad (16)$$

The eventual set of the two partial differential equations for e_1 and e_2 then is

$$\frac{\partial e_1}{\partial t} = \frac{1}{1+e_2} \frac{\partial}{\partial \omega} \left[C_e(e_1, e_2) \frac{\partial e_1}{\partial \omega} \right] + (1+e_1) q \quad (17)$$

$$\frac{\partial e_2}{\partial t} = - (1+e_2) q \quad (18)$$

in which

$$C_e = \frac{c_1 c_2 (1+e_0)^{c_2} d_a^2}{15\mu} \frac{e_1^{4.1}}{6 (1+e_1)^{4.1+c_2} (1+e_2)^{1+c_2}} \quad (19)$$

$$q = \frac{c_1 c_2 (1+e_0)^{c_2} d_c^2}{15\mu} \frac{e_2^{4.1}}{d_a (1+e_1)^{2+c_2} (1+e_2)^{3.1+c_2}} \left| \frac{\partial e_1}{\partial \omega} \right| \quad (20)$$

C_e is a type of diffusion coefficient, in the consolidation literature denoted as a modified consolidation coefficient.^{18,34} While this coefficient in a real-life expression process is varying with position and in time, in many papers,^{26,37} it is treated as a constant: this simplifies solving the consolidation equation which is a second-order partial differential equation. Kamst et al.,³⁰ however, appreciate the consolidation coefficient (also) depends on local cake porosity and compressibility. The review paper by Olivier et al.¹⁸ cites a number of authors (among which¹²) who all use similar relationships for diffusivity or consolidation coefficient. Our expression for C_e in Equation (19) is essentially different from earlier proposals due to the biporous character of our fat crystal slurry as a result of which it includes both the intraaggregate and the interaggregate solidosities. In addition, our consolidation equation, Equation (17), contains a source term which to the best of our knowledge is a novelty. Finally, our model looks much simpler than Lanoisellé's.

In more general terms, our expression model is a rheological model composed of two dashpots in series parallel to a spring. The double porous nature of the fat crystal aggregate filter cake is represented as a series of two dashpots, representative of some energy dissipation, described with the Meyer and Smith correlation for the permeability (rather than the Kozeny–Carman relation). The spring is due to the elastic modulus that can be determined experimentally with a constant load test.

6 | BOUNDARY AND INITIAL CONDITIONS

Solving the set of Equations (17) and (18) requires initial and boundary conditions for e_1 and e_2 . The material coordinate system, see

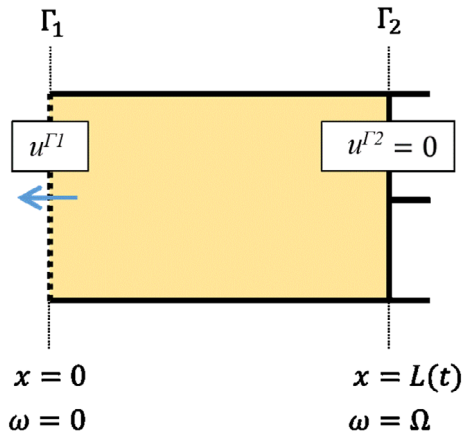


FIGURE 3 The domain of the expression with the cloth filter (taken infinitely thin) at the LHS and the pressure piston at the RHS, plus the notation and the two coordinate systems. Mind Equation (1): $d\omega = sdx$ [Color figure can be viewed at wileyonlinelibrary.com]

Equation (1), used in the expression model is illustrated in Figure 3. With this ω -coordinate, both boundaries are stationary. The position of the cloth at $\omega = 0$ is denoted by Γ_1 , while that of the piston at $\omega = \Omega$ is denoted by Γ_2 .

At Γ_2 , the liquid flux u always equals zero, implying that $\left. \frac{\partial p_l}{\partial x} \right|_{\Gamma_2} = 0$, thanks to Darcy's law, and therefore, as in Equation (20):

$$\left. \frac{\partial e_1}{\partial \omega} \right|_{\Gamma_2} = 0 \quad (21)$$

A similar Neumann boundary condition for u is applied at Γ_1 during the rest mode after the filling has been completed, resulting in similar boundary equation for e_1 at Γ_1 as Equation (21). The boundary condition for e_1 at Γ_1 during the filling mode and the pressing mode is found via the values for e_2 and e at Γ_1 thanks to

$$e_1^{\Gamma_1} = \frac{1 + e^{\Gamma_1}}{1 + e_2^{\Gamma_1}} - 1 \quad (22)$$

which follows from the expression for e in Table 1. We then need values for e_2 and e at Γ_1 , and—to find e , given Equations (8) and (15)—also values for the strain ε_{ls} and the pressure at Γ_1 . For the latter, we need the pressure drop Δp_c over the cake which due to Darcy's law relates to the piston pressure p_p applied at Γ_2 :

$$\Delta p_c = p_p \left(1 + \frac{R_f}{R_c} \right)^{-1} \quad (23)$$

in which R_f denotes the flow resistance of the filter cloth and R_c that of the cake which follows from

$$R_c = \int_0^L \frac{1}{k(x)} dx \quad (24)$$

The void ratio e_2 is a function of time only and therefore we need just an initial value for e_2 for the whole domain:

$$e_2(\omega, 0) = e_{2,0} = \frac{s_1^{rcp}}{s^{rcp}} - 1 \quad (25)$$

with s^{rcp} denoting the solid fat volume fraction at random close packing. The initial condition for e_1 runs as

$$e_1(\omega, 0) = e_{1,0} = \frac{\varepsilon_1^{rcp}}{s_1^{rcp}} \quad (26)$$

Finally, the total void ratio e_0 of the porous medium at the start of the expression step, needed in Equations (19) and (20), is related to s^{rcp} according to

$$e_0 = \frac{1 - s^{rcp}}{s^{rcp}} \quad (27)$$

7 | NUMERICAL IMPLEMENTATION

With the view of solving the two partial differential Equations (17) and (18) numerically, the 1D domain $[0, \Omega]$ (see Figure 3) is discretized into $J + 1$ nodes numbered with superscript j . Every node ω^j is assigned a length interval $[\omega^j - \frac{1}{2}\Delta\omega, \omega^j + \frac{1}{2}\Delta\omega]$, with $\Delta\omega = \Omega/J$. Half of the length interval associated with each of the two boundary nodes is inside the domain $[0, \Omega]$. To allow for imposing the above boundary conditions, one ghost node is added at either side of the domain, with indices $j = 1$ and $j = J + 3$, such that the plane $\omega = 0$ is in ω^2 and the plane $\omega = \Omega$ is in ω^{J+2} . The equations are solved with an Euler-forward finite-difference scheme implemented with MATLAB R2014b. To impose numerical stability in our explicit scheme, the time step Δt should obey the criterion

$$Fo_{\Delta} = \frac{C_{e0}\Delta t}{(\Delta\omega)^2} < \frac{1}{2} \quad (28)$$

where Fo_{Δ} is a local Fourier number and C_{e0} is a constant much larger than the maximum value of the consolidation coefficient C_e of Equation (19), that is, C_{e0} should be much larger than the constant factor in Equation (19).

The discretisation of Equations (17) and (18) is pretty straightforward. The same applies to the boundary conditions, except that for calculating a value of e_2 at node ω^2 (i.e., at $\omega = 0$) from Equations (18) and (20), a value of e_1 is needed at ghost node ω^1 . It is found by extrapolating from the e_1 values at nodes ω^2 , ω^3 and ω^4 by using equal ratios of differences between these nodes, given that the e_1 profile is found to be square root shaped. Care must be taken that the e_1 values at nodes ω^1 should not become negative. To realize the Neumann boundary condition at $\omega = \Omega$ by applying a central differencing scheme to

Equation (21), the value of e_1 at node $J + 3$ is taken equal to that at node $J + 1$. More details can be found in Hazelhoff Heeres' MSc thesis.³⁸

The time dependent filter cake thickness is calculated with

$$L^i = \Delta\omega \sum_{j=2}^{J+2} \omega_R^j (1 + e_1^{ij}) (1 + e_2^{ij}) \quad (29)$$

in which the superscript i denotes the time step of a variable and $\omega_R^j = 1$ unless $j = 2$ or $j = J + 2$: then it is $\frac{1}{2}$. The outflow velocity v_j^i through the filter cloth then follows from

$$v_j^i = \frac{L^{i-1} - L^i}{t^i - t^{i-1}} \quad (30)$$

8 | EXPERIMENTS

Of course, the above expression model was calibrated and validated by means of experimental results collected at pilot plant scale in a relatively small membrane filter press. It contained five filter plates making 4 filter chambers, each with 2 cross-flow areas of about 40 cm × 40 cm, creating 3 cm wide filter chambers. The flow resistance of the filter cloth was half a mm in thickness and made out of polypropylene. The edible fat crystal aggregate slurry was prepared in an on-site crystallizer and then pumped by a slurry pump into the filter chambers. The liquid produced during the expression process was collected in a bin standing on an electronic balance to register the flow rate.

Typically, some 20 kg of liquid was produced per experiment; depending on the manually controlled pressure profile imposed (rate of pressure increase, number of steps, duration of maximum pressure), this took between 10 and 15 min, the final maximum pressure in all cases being of the order of 5 bar(g) during some 5 min. Table 2 summarizes the conditions of 5 test runs all done on different days: tests #1 and #2 with a different edible fat batch than tests #3, #4, and #5. Figure 4 presents two pictures of filter cakes produced in the test rig. The final solid fat content of the cake was measured with a NMR analyzer. For the sake of our simulations, we take the (measured) solid fat content (which is on a mass basis) equal to the total solidosity in our

model (which is on a volumetric basis) due to ignoring density differences between oil and (liquid) fat.

9 | CALIBRATION OF THE MODEL

A straightforward validation of model predictions by means of experimental data collected in these tests is hampered by several experimental technicalities. First of all, as the model is 1D, it presumes a uniform composition of the medium in the other two directions and it ignores fluid motion and mixing, which certainly is not the case during the filling stage. A combined filtration and consolidation process already starts spontaneously during the filling of the filter chambers without any pressure being imposed.

The simulation of the expression starts as soon as in the filling stage the interaggregate porosity e_1 falls below e_1^{rcp} at the random close packing when the agglomerates start feeling they get compressed. In the tests, the filling is followed by a waiting period of some 20 s before the pressure is applied. In the simulations, this waiting period, or rest mode, is realized by imposing a zero outflow at Γ_1 . Then, pressure is applied and expression resumes resulting in a continued outflow. Another awkward technicality is that in the tests the separated liquid is staying behind in the tubing and piping between filter and collecting bin, while also the residence time in the collecting system leading to a retarded response of the balance is not in the model. A perfect match between model simulation and experiment is therefore not to be expected. We therefore carried out a calibration step first.

Table 3 presents model constants, physical properties, dimensions and simulation parameters used in both the calibration study and the validation study. The number of intervals J was selected after a sensitivity analysis with the view of balancing computational burden and accuracy. The flow resistance R_f of the filter cloth had been measured separately by filtering oil without solid fat. The value 0.228 for the solidosity s^{rcp} at random close packing was obtained by measuring the solid fat content of a cake in centrifugation experiments. The initial value e_0 follows from s^{rcp} thanks to Equation (27). In its turn, e_0 is used in estimating C_{e0} with Equation (19). The value 0.467 cm for Ω —see Figure 3—was found by measuring cakes from our pilot plant filtration/expression tests. The initial thickness L_0 of the filter cake was then back-calculated

TABLE 2 Summary of experimental conditions of 5 test runs for validation and calibration of the expression model

| Test # | Rate of pressure increase (bar/min) | Number of pressure steps | Duration of expression step, min |
|--------|-------------------------------------|--------------------------|----------------------------------|
| 1 | 1 | 1 | 10.5 |
| 2 | 0.5 | 1 | 15.2 |
| 3 | 1 | 3 | 13.5 |
| 4 | 1 | 3 | 11.8 |
| 5 | 1Q-sine | | 14.9 |

Note: The final pressure was the same in all 5 cases. In the tests with 3 pressure steps, pressure was held constant for a few minutes after each increase of 1 bar/min; 1Q-sine means a pressure versus time profile having the shape of a quarter of a sine.



FIGURE 4 Top view and side view of filter cakes produced in the pilot plant filter press. The membrane side is up. The thickness of the cakes is almost 25 mm [Color figure can be viewed at wileyonlinelibrary.com]

TABLE 3 Summary of parameters used in the simulations with the expression model

| Quantity | Value | Units | Equation |
|----------------|----------------------|----------|----------|
| c_1 | 3.31 | kPa | (15) |
| c_2 | 5.18 | - | (15) |
| C_{e0} | 10^{-5} | m^2/s | (28) |
| ρ | 910 | kg/m^3 | |
| μ | 0.06 | Ns/m^2 | |
| d_c | 2 | μm | (20) |
| R_f | 1.6×10^{-9} | m^{-1} | (23) |
| L_0 | 2.05 | cm | |
| s^{rcp} | 0.228 | | (25) |
| Ω | 0.467 | cm | (1) |
| J | 23 | - | |
| $\Delta\omega$ | 0.203 | mm | |
| Δt | 2.1 | ms | (28) |

from Ω and the above value of s^{rcp} by using $\Omega = s^{rcp} L_0$ which reflects Equation (1) and the above value of s^{rcp} , in an attempt to correct for the loss of liquid in the first phase of the filling stage with outflow without pressure being applied yet.

However, the model contains three more parameters we actually do not know from the onset, viz. (a) the aggregate diameter d_a occurring in Equations (19) and (20), (b) the interaggregate solidosity s_1^{rcp} at random close packing, needed to calculate the initial values $e_{1,0}$ and $e_{2,0}$ with Equations (25) and (26), and (c) the solid fat content, or total solidosity s , at the start of the expression process.

In addition, it turns out that, even with reasonable guesses for these three parameters, the outflow velocity calculated with Equation (30) cannot be made to match the outflow as measured in the tests. The way out was to introduce two so-called flow resistance factors, denoted by a_1 and a_2 , with the view of reducing the values of consolidation coefficient C_e and release rate q , see Equations (19) and (20), by dividing them by a_1 and a_2 ,

respectively. Tests 1 and 2 were then used to calibrate the expression model by systematically varying the above five parameters within physically plausible ranges. Figure 5 presents for these two tests the comparison between simulated and experimental outflows as a function of time. The legends also show the R^2 values which indicate a match which per test is very good.

The two sets of optimized coefficients differ quite a bit, while the only difference between the two tests is in the rate of pressure increase. The discrepancies between the two sets may illustrate the challenge of dealing with the experimental technicalities. The best thing to do was to average the two sets to produce the following set which will be used for the remainder of the tests of this paper:

$$a_1 = 2.7 \quad a_2 = 42 \quad d_a = 230 \mu m \quad s_1^{rcp} = 0.59 \quad SFC_{0,p} = 0.35 \quad (31)$$

The flow resistance factor $a_1 = 2.7$ may be related to an over-prediction of cake permeability k_1 by Equation (14): our own experiments showed an over-prediction by a factor of 5. This also affects consolidation coefficient, see Equation (19). The value 42 for the flow resistance factor a_2 may be due an over-estimation of both agglomerate permeability k_2 and crystal diameter d_c (which occurs squared). The value 0.59 for the inter-aggregate solidosity s_1^{rcp} looks a bit low, where Torquato et al.,³⁹ in a molecular dynamics study of hard spheres, report a packing fraction of 0.64 for a maximally random jammed state.

Figure 6 shows a comparison of simulation results obtained with the set of optimized coefficients of Equation (31) and experimental outflow velocities for the same tests #1 and #2 as above. Compared to Figure 5, the agreement falls a bit short, with lower values for R^2 .

10 | VALIDATION OF THE MODEL

The other three tests of Table 2, carried out with a different edible fat batch, were used for validating the expression model including the coefficient of Equation (31). The results for the outflow velocity

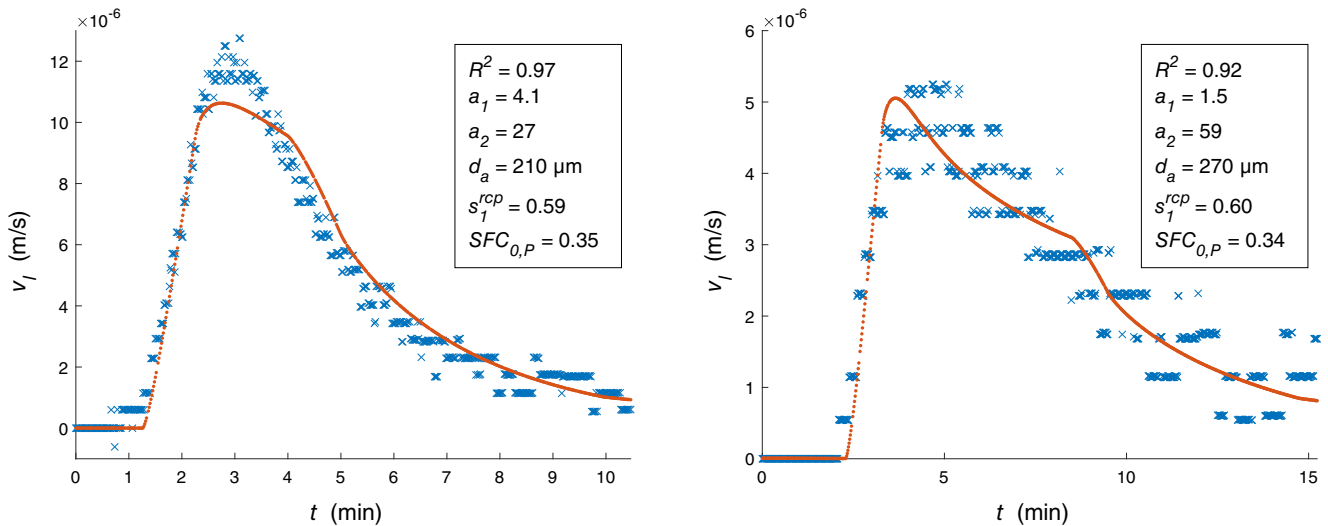


FIGURE 5 Comparison of simulated (red line) and experimental (blue crosses) outflow velocities in test #1 (left) and test #2 (right) where the simulations were calibrated by use of optimized values for the five parameters mentioned in the legends [Color figure can be viewed at wileyonlinelibrary.com]

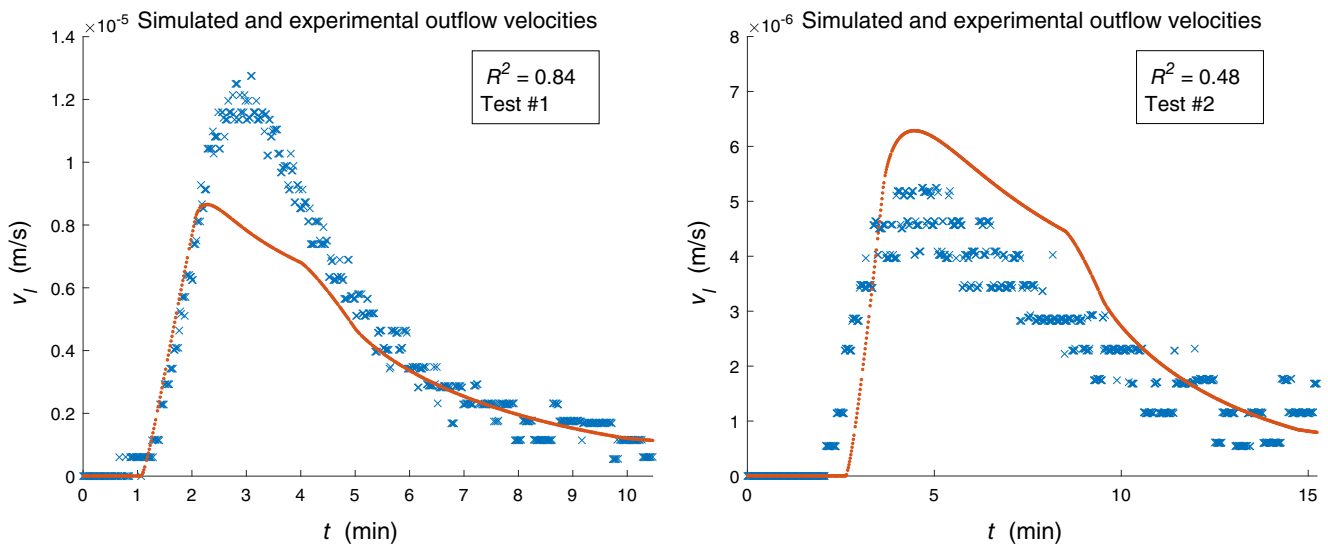


FIGURE 6 Comparison of simulated (red line) and experimental (blue crosses) outflow velocities in test #1 (left) and test #2 (right) where the simulations were calibrated by use of the averaged optimized values for the five parameters mentioned in Equation (31) [Color figure can be viewed at wileyonlinelibrary.com]

profiles are shown in Figure 7. Tests 3 and 4 are just duplicates, with an identical simulated velocity profile, although test #4 was stopped earlier than #3, and again show the spread in experimental results due to the technicalities described above. In addition, the manual control of the pressure profile adds to the spread. Note that in both tests #3 and #4, the pressure increase was interrupted twice (see Table 2), the first time at the rather low pressure of 1 bar (g) that was maintained for a few minutes; in the simulations this obviously did not result in an outflow. The agreement between simulation and test is far better again in test #5 where, just like in tests

#1 and #2, pressure was increased continuously (though in an different way) up to the same final maximum pressure.

11 | FILTER CAKE COMPOSITION AND PROFILE

Given the satisfactory results of the calibration study, which was restricted to the outflow velocity through the membrane, we now present the model's findings with respect to the spatial and temporal

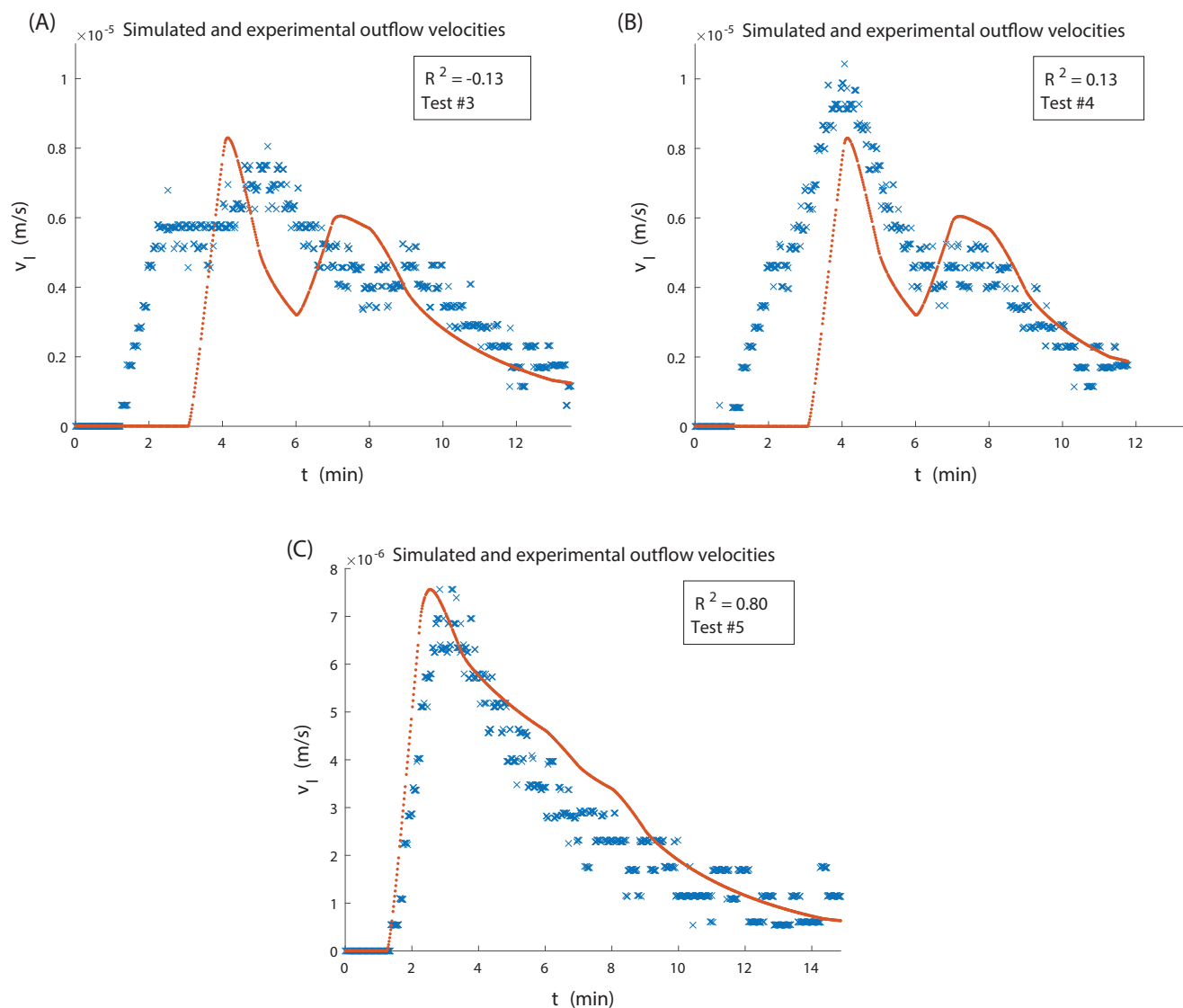


FIGURE 7 Comparison of simulated (red line) and experimental (blue crosses) outflow velocities in tests #3, #4, and #5, simulations having been run with the five optimized parameters mentioned in Equation (31) [Color figure can be viewed at wileyonlinelibrary.com]

evolution of the filter cake composition which lies at the basis of the outflow velocity. Figure 8 presents a typical result, for test #1, in terms of the volume fractions ε_1 (the interagglomerate liquid), $\varepsilon_2 s_1$ (the intraagglomerate liquid) and the total solidosity $s_2 s_1 (=s)$. Each of these three volume fractions which add up to unity, has been colored with a different shade of ochre. Each panel of Figure 8 shows, for a specific moment in time, the composition of the cake as a function of x (translated from ω). The upper curves in the four panels exhibit the typical propagating error function shape associated with transient diffusion, with penetration time of the order of 0.2 min (viz., $L_0^2/\pi C_{e0}$), while three of the four lower, ε_1 , curves are rather flat, indicating the release of fat from the agglomerates is rate limiting for the fat separation through the filter cloth. This is due to the second-order diffusion equation for ε_1 while ε_2 obeys a simple mass balance. The total thickness of the filter cake decreases over time as indicated by the position of the piston. This decrease clearly slows down as permeability

decreases over time, see Equation (14), while the elastic modulus increases, see Equation (16).

Figure 9 illustrates that the (average) eventual solid fat content found in the simulations is in very good agreement with the experimental data, certainly given the uncertainty (represented by the error bars) in both experiments and simulations. The error bars of the simulations are based on differences found in simulations with different sets of calibration coefficients, such as in Figures 5 and 6. The experimental uncertainty is once more clear from the different values of the solid fat content of the similar tests #3 and #4: test #4 was stopped earlier than #3 and therefore should contain more oil indeed (as in the simulations), while this was not observed in the tests. In test #5, the average solid fat content was predicted too high while the outflow simulation (see Figure 7) was very well predicted.

Finally, we checked whether the simulation reproduces the solid fat profile in the eventual filter cake as found in the pilot-plant tests. To

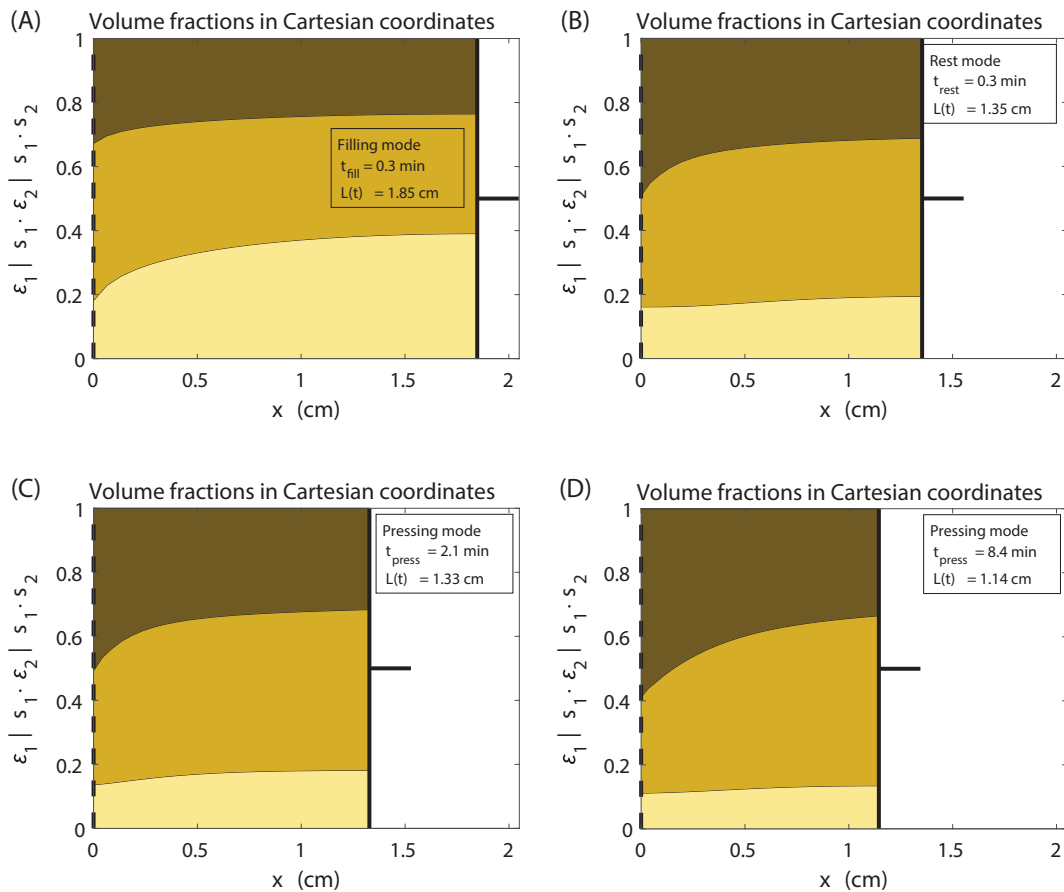


FIGURE 8 Volume fractions vs. position in the cake as calculated by our model with the set of coefficients of Equation (31) for test #1. The position of the filter cloth on the left is fixed. The total thickness of the filter cake decreases over time. The lower region represents ϵ_1 (the interagglomerate liquid), the middle one $\epsilon_2 s_1$ (the intraagglomerate liquid) and the upper one is total solidosity $s_2 s_1 (=s)$. The times t_{fill} , t_{rest} , and t_{press} denote the times passed since the start of the filling, rest, and pressing modes, respectively [Color figure can be viewed at wileyonlinelibrary.com]

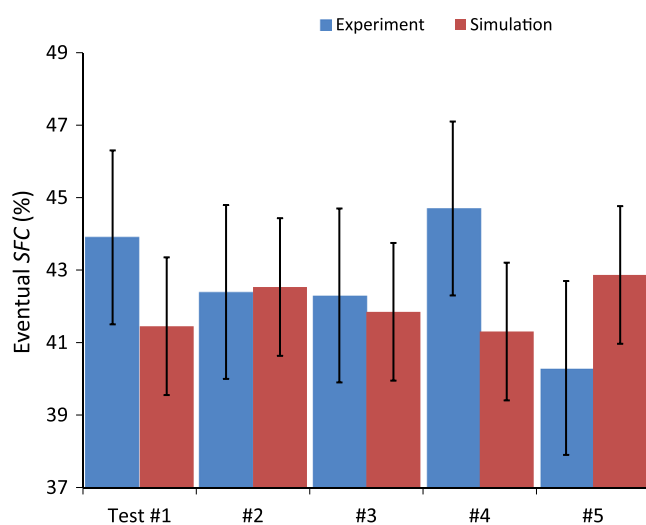


FIGURE 9 Final solid fat content for all 5 cases: comparison between experiment (blue, left) and simulation (purple, right) [Color figure can be viewed at wileyonlinelibrary.com]

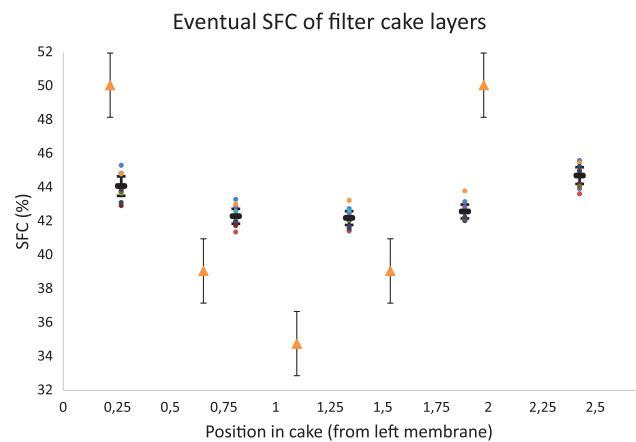


FIGURE 10 The final solid fat content in test #2 as a function of position in the filter cake. The five triangles denote the simulation results, while the test results are represented by the overlapping symbols. The uncertainty in the simulation data has been estimated from a number of simulations with varying calibration coefficients [Color figure can be viewed at wileyonlinelibrary.com]

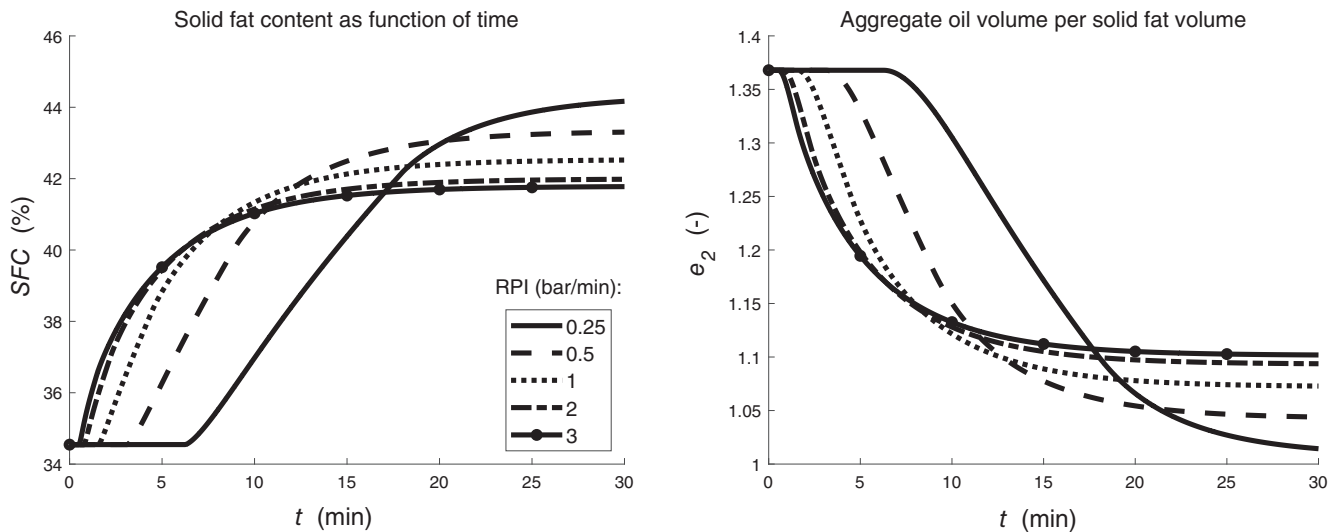


FIGURE 11 Solid fat content (SFC, left) and pore volume per solid fat volume (right) as a function of expression time, for various RPIs (rates of pressure increase) in the range 0.25–3 bar/min

this end, the filter cake produced in test #2 was removed from the filter chamber and sliced with the help of an egg slicer into five layers of approximately equal thickness. This is a tedious operation, as oil dripped on the cake during removal and cutting was difficult, with the cake easily crumbling and melting during handling. The solid fat content of 10 samples out of each slice was measured and averaged to construct a profile of solid fat content versus position in the cake. Something similar, though for three slices, was done after completion of the pertinent simulation. In the tests in the membrane filter press, the cake was contained between two membranes, while in the simulation there was just a single membrane (at the left-hand side). For the sake of the comparison in Figure 10 the computed profile was mirrored. As expected, the solid fat concentration is minimum in the middle of the cake in both test and simulation. Note that the final thicknesses of the cake in the test (24.3 mm) and in the mirrored simulation (2×11.4 mm) are not exactly the same, since—due to the technicalities mentioned earlier with respect to the start of the expression stage—also the initial cake thicknesses were taken different. Given the experimental inaccuracies and the simplifications of the 1D model, the difference between the two curves is surprisingly good.

12 | APPLICATION OF THE MODEL

The interest of companies is in producing a high edible fat content in a period as short as possible. This translates into questions as to which final pressure level, which pressure–time profile (including the option of increasing pressure in steps) and which duration of the process are optimum. The expression model reported in this paper could be helpful in deciding on these issues. To illustrate the potential of the model, we investigated the effect of varying the constant rate of pressure increase on the eventual solid fat content, the final pressure level being kept the same.

Figure 11 illustrates, for various rates of pressure increase, how solid fat content increases in time due to a decrease in e_2 denoting pore volume (or aggregate oil) per solid fat volume which is constant over time. Equations (12) and (13) tell us that the decrease in e_2 depends on the gradient in e_1 . A slower pressure increase implies that it takes longer for the gradient in e_1 to vanish and for the filter cake to obtain an equilibrium state. It also takes longer to reach the final pressure level partly because the squeezing and the oil separation set in later in time, but it results in a higher solid fat content (some 2%). In spite of the limitations and uncertainties of our 1D filtration model, these results at least suggest our model may successfully be used for ranking process options. We like to emphasize that our experience with tests in a pilot-plant scale membrane filter press suggest that such a ranking exercise is harder, and more expensive, on the basis of tests, due to inevitable slight variations between tests in slurry composition and properties, a range of equipment and operational issues discussed earlier, and the relatively large uncertainties in the measurements.

13 | CONCLUSIONS

A 1D pressure filtration model for edible fats, focusing on the expression step, has been developed and described. The model comprises two differential equations one of which is a second-order diffusion equation with a nonconstant consolidation coefficient while the second is a simple transient mass balance. The expression we derived for this consolidation (or diffusion) coefficient is essentially different from earlier proposals in the literature since we explicitly take the biporous character of our fat crystal slurry into account, in terms of intraaggregate and interaggregate solidosities. In addition, our consolidation equation contains a source term which to the best of our

knowledge is a novelty. In general terms, our set of two differential equations represents a rheological model composed of a series of two dashpots parallel to a spring. The double porous nature of the fat crystal aggregate filter cake can be conceived as a series of two dashpots described with the Meyer and Smith correlation for the permeability (rather than the Kozeny–Carman relation). The spring is due to the elastic modulus that can be determined experimentally with a constant load test.

The model was implemented in MATLAB with five unknown coefficients remaining, which were calibrated with the help of measured oil outflow rates in two filtration tests in a pilot scale membrane filter press. The model was then validated by using experimental data from five filtration tests. The model is capable of displaying porosities and solidosities, the solid fat content inclusively, as a function of time and of position in the filter cake. In addition, it can generate plots of overall features of the filtration process such as oil outflow velocity, solid fat content of the filter cake and aggregate oil volume, all as a function of time.

The overall conclusion is that the model gives very promising results, qualitatively realistic and obviously pretty reliable, with room for improvement in quantitative respect. Our simulations may also result in process information which is more consistent than data from pilot plant tests which suffer from several equipment technicalities and operational issues. Specific experiments may be helpful to find more reliable and accurate data for some cake features such as permeability and elasticity as a function of particularly aggregate properties of typical edible fats.

Finally, the model has been shown to have the potential of exploring the effect of typical process operation variables on eventual solid fat content of the filter cake, such as the rate of pressure increase and, related, the duration of the expression phase.

ACKNOWLEDGMENTS

The challenge of developing a better expression model was given to a team of PhD students from Dutch Physics Departments in the context of a week-long Physics for Industry event organized by the Dutch research foundation FOM in Fall 2015. The arrangements made by FOM are highly appreciated. In this week, the basis was laid for the model described in this paper which resulted from the MSc final year research project of the second author. The authors acknowledge the practical guidance in lab and pilot plant trials by Richard van Leeuwen, Johan Draisma and Hanung Sonneveld, all FrieslandCampina.

AUTHOR CONTRIBUTIONS

Harry Van den Akker: Conceptualization; formal analysis; funding acquisition; investigation; methodology; resources; supervision; validation; writing-original draft; writing-review & editing. **Doedo Hazelhoff Heeres:** Formal analysis; investigation; methodology; software; validation. **William Kloek:** Conceptualization; formal analysis; funding acquisition; investigation; methodology; resources; supervision; validation.

DATA AVAILABILITY STATEMENT

A more elaborate report of this research can be found in the final-year research report of MSc student Doedo Hazelhoff Heeres (Ref. 38) available at <https://repository.tudelft.nl/>. Further data (mainly on the experiments) may be available from the authors on request.

ORCID

Harry E. A. Van den Akker  <https://orcid.org/0000-0002-8143-5895>

REFERENCES

- Xu YM, Dabros T, Kan JM. Filterability of oil sands tailings. *Process Saf Environ Protect*. 2008;86(B4):268-276.
- Angle CW, Clarke B, Dabros T. Dewatering kinetics and viscoelastic properties of kaolin as tailings model under compressive pressures. *Chem Eng Res Des*. 2017;118:286-293.
- Raman GSS, Klima MS. Evaluation of pressure filtration of coal refuse slurry: a fractional factorial design approach. *Int J Coal Preparat Util*. 2019;39(6):332-344.
- LaHeij EJ et al. Fundamental aspects of sludge filtration and expression. *Water Res*. 1996;30(3):697-703.
- Ramarao BV, Lavrykov S, Tien C. Nonequilibrium compression effects in the dewatering of fibrous suspensions: analysis using dual porosity dual permeability approach. *AIChE Annual Meeting*. OH, USA: Cincinnati; 2005.
- Abdud MY et al. Experimental and modelling studies on the solvent assisted hydraulic pressing of dehulled rubber seeds. *Ind Crop Prod*. 2016;92:67-76.
- Arslan N, Kar F. Filtration of sugar-beet pulp pectin extract and flow properties of pectin solutions. *J Food Eng*. 1998;36(1):113-122.
- Chai ZH, Zhao TS. A pseudopotential-based multiple-relaxation-time lattice Boltzmann model for multicomponent/multiphase flows. *Acta Mech Sin*. 2012;28(4):983-992.
- Venter MJ, Kuipers NJM, de Haan AB. Modelling and experimental evaluation of high-pressure expression of cocoa nibs. *J Food Eng*. 2007;80(4):1157-1170.
- Mrema GC, McNulty PB. Mathematical model of mechanical oil expression from oilseeds. *J Agric Eng Res*. 1985;31(4):361-370.
- Ocenasek J, Voldrich J. Mathematical modelling of biogenous filter cake and identification of oilseed material parameters. *Appl Comput Mech*. 2009;3(2):339-350.
- Stickland AD, De Kretser RG, Scales PJ. Nontraditional constant pressure filtration behavior. *AIChE J*. 2005;51(9):2481-2488.
- Terzaghi K. Die Berechnung der Durchlässigkeitsziffer des tones aus dem Verlauf der Hydrodynamischen Spannungserscheinungen (a method of calculating the coefficient of permeability of clay from the variation of hydrodynamic stress with time). *Akad Wissenschaft Wien, Math-Naturwiss Klasse*. 1923;132:125-138. See also: Proc. Instn. Civil Engrs. Geotech. Engng., 1995, 113, 191-205.
- Ruth BF. Studies in filtration. III. Derivation of general filtration equations. *Ind Eng Chem*. 1935;27:708-723.
- Carman PC. Fluid flow through granular beds. *Trans IChemE*. 1937;15: 150-166.
- Barenblatt GI, Zheltov IP. Fundamental equations for the filtration of homogeneous fluids through fissured rocks. *Dokl Akad Nauk SSSR*. 1960;132(3):545-548.
- Chen ZX. Transient flow of slightly compressible fluids through double-porosity, double-permeability systems—a state of the art review. *Transport Porous Media*. 1989;4(2):147-184.
- Olivier J, Vaxelaire J, Vorobiev E. Modelling of cake filtration: an overview. *Sep Sci Technol*. 2007;42(8):1667-1700.
- Tien C. *Introduction to Cake Filtration*. Amsterdam: Elsevier; 2006.
- Tien C. *Principles of Filtration*. Amsterdam: Elsevier; 2012.

21. Mahwachi M, Mihoubi D. Pressure and porosity profiles during filtration-expression process. *Theor Found Chem Eng.* 2020;54(2):370-379.
22. Tiller FM, Cooper HR. The role of porosity in filtration. 4. Constant pressure filtration. *AIChE J.* 1960;6(4):595-601.
23. Tiller FM, Shirato M. The role of porosity in filtration 6. New definition of filtration resistance. *AIChE J.* 1964;10(1):61-67.
24. Landman KA, White LR. Predicting filtration time and maximizing throughput in a pressure filter. *AIChE J.* 1997;43(12):3147-3160.
25. Owolarafe OK et al. Mathematical modelling and simulation of the hydraulic expression of oil from oil palm fruit. *Biosyst Eng.* 2008;101(3):331-340.
26. Shirato M et al. Fundamental studies of expression under variable pressure. *J Chem Eng Jpn.* 1970;3(1):105-112.
27. Buttersack C. 2-zone model for solid-liquid separation by filtration and expression. *Chem Eng Sci.* 1994;49(8):1145-1160.
28. Lanoiselle JL et al. Modeling of solid/liquid expression for cellular materials. *AIChE J.* 1996;42(7):2057-2068.
29. Petryk M, Vorobiev E. Numerical and analytical modeling of solid-liquid expression from soft plant materials. *AIChE J.* 2013;59(12):4762-4771.
30. Kamst GF, Bruinsma OSL, de Graauw J. Permeability of filter cakes of palm oil in relation to mechanical expression. *AIChE J.* 1997;43(3):673-680.
31. Kamst GF, Bruinsma OSL, de Graauw J. Solid-phase creep during the expression of palm-oil filter cakes. *AIChE J.* 1997;43(3):665-672.
32. Tien C, Ramarao BV. Can filter cake porosity be estimated based on the Kozeny-Carman equation? *Powder Technol.* 2013;237:233-240.
33. Smiles DE. Use of material coordinates in porous media solute and water flow. *Chem Eng J.* 2000;80(1-3):215-220.
34. Sorensen PB, Moldrup P, Hansen JAA. Filtration and expression of compressible cakes. *Chem Eng Sci.* 1996;51(6):967-979.
35. Tosun I. Formulation of cake filtration. *Chem Eng Sci.* 1986;41(10):2563-2568.
36. Meyer BA, Smith DW. Flow through porous media—comparison of consolidated and unconsolidated materials. *Ind Eng Chem Fund.* 1985;24(3):360-368.
37. Andersen NPR, Christensen ML, Keiding K. New approach to determining consolidation coefficients using cake-filtration experiments. *Powder Technol.* 2004;142(2-3):98-102.
38. Hazelhoff Heeres, D.P., *Pressure filtration of milk fat slurries* (MSc thesis, Faculty of Applied Sciences, Department of Chemical Engineering). Delft University of Technology: Delft; 2018.
39. Torquato S, Truskett TM, Debenedetti PG. Is random close packing of spheres well defined? *Phys Rev Lett.* 2000;84(10):2064-2067.

How to cite this article: Van den Akker HEA, Hazelhoff Heeres DP, Kloek W. A spatially resolved model for pressure filtration of edible fat slurries. *AIChE J.* 2021;e17307. <https://doi.org/10.1002/aic.17307>